Energy & Buildings 357 (2026) 117163

Contents lists available at ScienceDirect

Energy & Buildings

journal homepage: www.elsevier.com/locate/enb

Summer thermal consequences of EU retrofit Strategies: An integrated microclimate and indoor comfort study in Düsseldorf☆

Qinghua Yu [a,*], Gerald Mills [b], Gunnar Ketzler [a], Michael Leuchner [a]

[a] Physical Geography and Climatology, Institute of Geography, RWTH Aachen University, Aachen, Germany
[b] School of Geography, University College Dublin, Dublin, Ireland

ARTICLE INFO

Keywords:
ENVI-met
CitySim
Building archetypes
Buildingretrofit
UTCI
Urban microclimate

ABSTRACT

Building retrofits in temperate European climates primarily target winter heat losses, yet their dynamic implications for outdoor microclimate and indoor thermal safety under heatwaves remain poorly understood. This study investigates how winter-oriented retrofits modify both outdoor microclimate and indoor thermal conditions during July 2022 Central European heatwaves, using a one-way, offline integration of ENVI-met and CitySim. A dense residential neighborhood in Düsseldorf, Germany, was simulated under multiple retrofit and greening scenarios, incorporating realistic building data derived from the EU TABULA archetype database to ensure reliable façade–microclimate interactions.

Methodologically, results show that using realistic archetypes alters simulated outdoor heat stress by up to 1.5 °C compared to generic defaults. In terms of mitigation, façade retrofits alone slightly reduce outdoor Universal Thermal Climate Index (UTCI) by up to 0.8 °C, while green infrastructure provides the strongest cooling, lowering local UTCI by up to 6 °C through shading and evapotranspiration. Typically, indoor simulations revealed a crossover effect, where retrofitted buildings remained cooler at night but became up to 3.8 °C warmer during daytime peaks, increasing short-term overheating risks in the absence of active cooling.

These findings highlight a mitigation–adaptation trade-off in EU retrofit strategies: measures optimized for winter energy savings can exacerbate summer heat stress if not combined with greenery and summer-oriented design measures. The proposed framework offers a scalable workflow to support climate-resilient, human-centric retrofit planning in other TABULA-covered cities.

1. Introduction

Rapid urbanization and the densification of cities have intensified the modification of natural land surfaces, replacing them with impervious materials such as asphalt and concrete [1]. These changes, coupled with increased anthropogenic heat emissions from transportation and buildings, have contributed to the intensification of the urban heat island (UHI) effect [2]. UHI exacerbates urban energy demand for cooling [3], deteriorates air quality [4] and increases heat-related health issues during periods of extreme heat [5]. At the local scale, UHI also intensifies the impacts of more frequent and severe heatwave events [6]. Recent studies report substantial excess mortality during heatwaves in different regions, and during summer 2022 Europe experienced particularly severe impacts, including several thousand heat-related deaths in Germany alone [7]. These figures highlight the need for urban environments that limit both outdoor thermal exposure and indoor overheating during persistent heatwaves.

Most existing urban heat mitigation strategies focus on the use of green infrastructure (trees, parks, green roofs/façades) and reflective or high-albedo materials to improve outdoor thermal comfort [8–11]. Meanwhile, a growing body of work has examined advanced energy-efficiency and retrofit technologies, including alternative envelope configurations and façade photovoltaic systems, primarily targeting reductions in heating demand and operational carbon emissions [12,13]. Building- and room-scale studies have also developed sophisticated monitoring and control approaches, including mobile thermal-comfort monitoring robots, demand-side energy management for HVAC, and reinforcement-learning-based optimal ventilation strategies to balance energy use, indoor air quality and thermal comfort [14–16]. However, far less attention has been paid to the unintended summer

☆ This article is part of a special issue entitled: 'ENB_Low-Carbon Comfort-Centric Buildings' published in Energy & Buildings.

* Corresponding author.
E-mail address: qinghua.yu@geo.rwth-aachen.de (Q. Yu).

https://doi.org/10.1016/j.enbuild.2026.117163
Received 8 October 2025; Received in revised form 8 February 2026; Accepted 12 February 2026
Available online 13 February 2026
0378-7788/© 2026 The Author(s). Published by Elsevier B.V. This is an open access article under the CC BY license (http://creativecommons.org/licenses/by/4.0/).

consequences of winter-driven building retrofit measures.

In much of Western and Central Europe, where temperate oceanic climates dominate (Cfb in the Köppen classification) [17], the historical climate focus has been on cold stress in winter rather than summer overheating. Düsseldorf, with comparatively mild but warming summers and still cold winters, provides a representative Central European testbed for examining these trade-offs. At the same time, a substantial share of the residential building stock predates the first German thermal insulation ordinance in 1978, indicating considerable potential for energy retrofits [18]. Consequently, most retrofit strategies have emphasized improving insulation and reducing heat loss [19]. One such popular housing retrofit project is the EU TABULA project (Typology Approach for Building Stock Energy Assessment) [20], which developed comprehensive national building typologies and retrofit strategies across 20 European countries, focusing primarily on improving winter energy performance.

The European Green Deal's Renovation Wave and the recast Energy Performance of Buildings Directive (EPBD) aim to at least double renovation rates by 2030 and steer the building stock towards very low or zero operational emissions by 2050 [21]. Current strategies for winter energy-saving home retrofits mainly quantify benefits in terms of energy savings, emissions reduction and affordability, while explicit treatment of summer thermal comfort and heat–health resilience remains limited [19]. Concurrently, studies from the perspective of governance and equity have highlighted that carbon reduction policies may exacerbate inequality if structural constraints are disregarded [22]. Together, these developments underline the need to assess not only the mitigation benefits of standard retrofit packages, but also their implications for thermal comfort and heat-health resilience.

In light of intensifying and more frequent heatwaves in Europe, it is crucial to investigate whether building retrofits designed for winter performance might compromise summer thermal safety, both indoors and outdoors. This study addresses that gap by using a real-world case in Düsseldorf, Germany to evaluate the microclimatic and thermal effects of EU-standard retrofit strategies under extreme summer heatwave conditions.

In earlier work, Yu et al. [23] developed an urban geographic archetype dataset and applied it to Düsseldorf's residential buildings using the Urban Building Energy Model (UBEM), CitySim [24]. That work demonstrated that standardized retrofitting strategies could reduce annual CO_2 emissions by 42–46% and lower heating energy demand by around 70% by 2050. However, those simulations were winter-oriented and did not explore potential trade-offs during summer. Moreover, CitySim's simplified climate inputs and lack of vegetation modeling limited its ability to represent the complex interactions between building surfaces and the urban microclimate [25].

To bridge this gap, we linked ENVI-met [26] and CitySim in the same neighborhood through a one-way, offline integration scheme. ENVI-met enables simulation of surface–atmosphere interactions, capturing how vegetation, urban morphology, and façade properties influence outdoor comfort as quantified by the Universal Thermal Climate Index (UTCI) [27]. CitySim is used to simulate indoor operative temperatures in buildings, using the same construction properties. In a novel step, we replaced CitySim's default weather profiles with high-resolution, scenario-specific microclimate data extracted from ENVI-met outputs. This cross-model linkage allowed us to evaluate how building retrofit decisions shape both indoor and outdoor thermal performance under extreme summer conditions.

Yu et al. [28] reviewed recent integrative microclimate-building studies, finding that most of integration are sequential from microclimate to building energy approaches, such as ENVI-met–CEA and ENVI-met–TRNSYS workflows, used to examine the combined effects of urban form, greenery and building operation on energy demand and outdoor comfort [29,30]. More recent works published between 2023 and 2025 have extended such integrations to different climates and design questions [31,32]. However, even when these studies include site-specific validation, they typically rely on simplified or generic urban morphologies and thermophysical properties and often treat "retrofits" as idealized parameter variations. To fill this gap, a further innovation of this study is the use of detailed, archetype-based building information for both simulation environments. We investigated how realistic, archetype-based building data influences modeled UTCI and thermal comfort outcomes. This study does not attempt a new, site-specific validation of ENVI-met or CitySim against local measurements in Düsseldorf. Instead, we build on existing validation studies of both models and focus on how building envelope realism affects the simulated magnitude and spatial distribution of outdoor heat stress, and the associated indoor responses under extreme conditions.

To fill the existing research gap in linking retrofit-driven envelope modifications with outdoor–indoor thermal responses, this study addresses the following questions:

(1) To what extent does the use of realistic building data influence the magnitude and spatial distribution of simulated outdoor thermal comfort outcomes compared to generic default settings under extreme heat conditions? (2) Can energy retrofit measures focused on winter performance unintentionally worsen outdoor comfort and increase daytime indoor overheating risk by a threshold amount (e.g., >3.0 °C) during summer heatwaves? (3) How effectively can the integration of green infrastructure with building retrofits reduce peak UTCI and alleviate indoor overheating during summer heatwaves?

The core achievements of this study are threefold. First, we developed a transparent, data-driven ENVI-met–CitySim framework with a one-way, offline integration that consistently applies EU TABULA archetype data across both microclimate and building energy simulations. Second, we provide a quantitative, dual-domain assessment of a critical policy trade-off, revealing a crossover effect where winter-optimized retrofits significantly increase the risk of daytime indoor overheating by up to 3.8 °C during heatwaves, while only moderately improving outdoor comfort. Third, we confirm the essential role of nature-based solutions, demonstrating that integrating green infrastructure is the single most effective strategy for localized heat mitigation, capable of reducing UTCI by up to 6.0 °C in shaded areas.

Beyond the specific case of Düsseldorf, the proposed integrated modeling framework provides a scalable and transferable evaluation tool for integrating retrofit policy design to other European cities covered by the TABULA database, human-centric comfort, and low-carbon objectives in future climate-resilient building programs.

2. Methodology

2.1. Study area

The study area is located in Düsseldorf, Germany, the seventh-largest city in the country, with a population of over 600,000 residents [33]. Düsseldorf experiences a temperate climate with distinct seasonal variability, with the mean annual temperature over the standard 1991–2020 climate normal period of approximately 11.2 °C. During the summer, the city experiences a moderate number of summer days, where maximum temperatures reach or exceed 25 °C, usually ranging from 15 to 26 days per year. Hot days, where temperatures reach or exceed 30 °C, are relatively rare. Winters are often cold, with frost days (minimum temperatures below 0 °C) frequently occurring, sometimes reaching up to 90 days annually [34]. Historically, the city has been more concerned with winter cold stress than extreme summer heat. Fig. 1 shows the geographic location of Düsseldorf in Germany and the location of the meteorological station at Düsseldorf Airport.

The case study area is situated in Düsseldorf's Flingern district, consisting of three blocks and one street park (Fig. 2). The buildings are predominantly residential, with some mixed-use buildings serving as small workshops, offices, and schools. The layout follows a typical German block design, where buildings along the major roads are taller, while elsewhere there are low-rise terraced houses [35]. In this study

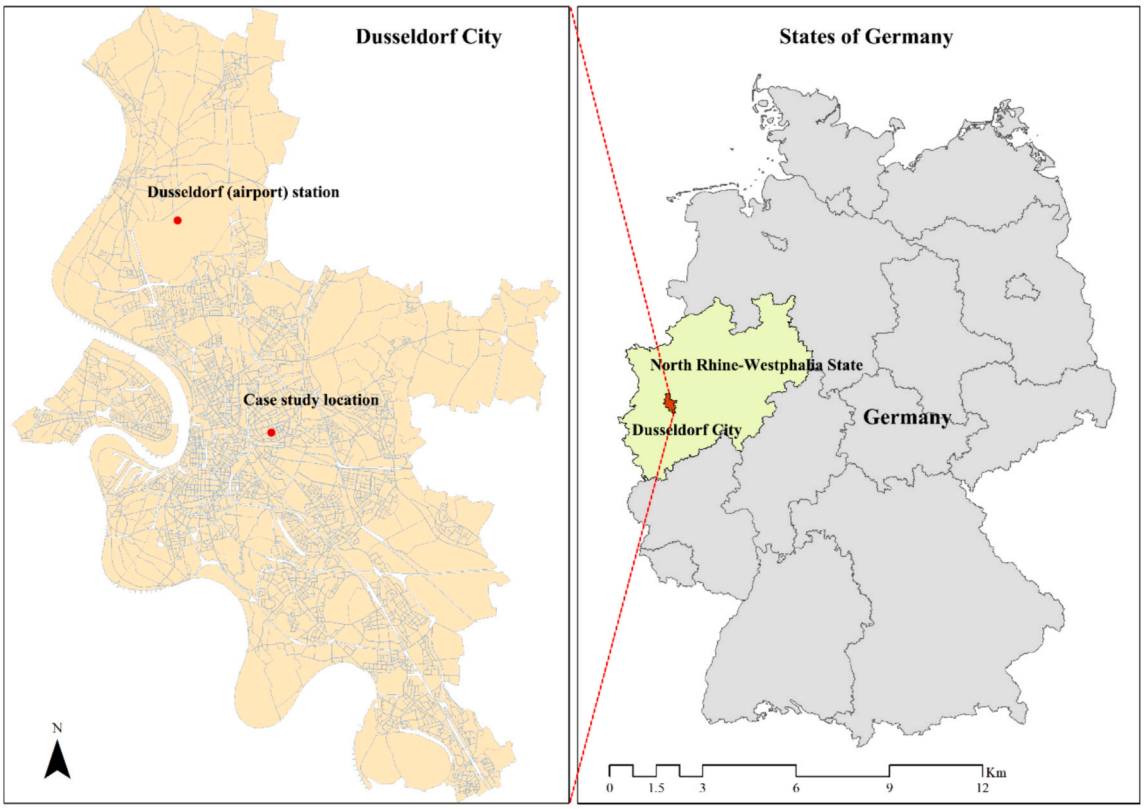


Fig. 1. The location of the research area and meteorological station in Düsseldorf (left). Location of the city and North Rhine-Westphalia in Germany (right).



Fig. 2. Different land covers are divided into seven classes, namely, asphalt red pavement, asphalt pavement, single stones pavement, concrete pavement, building, grass and soil. The locations of trees are also shown in the map [50]. The red line indicates the area of interest for model simulations. (For interpretation of the references to colour in this figure legend, the reader is referred to the web version of this article.)

area, the average height of periphery buildings of each block is 21 m, while for the interior building of the blocks it is 5 m. Fig. 2 shows building heights in 10-meter intervals as two classes. The street park, cutting through the center of the research area, offers environmental and social amenities. The total study area is approximately 34.26 ha, including 44% paved roads and walkways, 37% buildings and 19% green ground cover (lawns, gardens).

2.2. Outdoor microclimate simulation with ENVI-met

To examine the effect of retrofitting strategies on outdoor thermal comfort, we used ENVI-met (v5.5.1), which is a three-dimensional, non-hydrostatic microclimate model designed to simulate surface–plant–air interactions in urban environments at high spatial and temporal resolutions [26]. It is widely used for assessing the effects of urban design strategies, such as vegetation, materials, and building geometry on local thermal comfort and microclimate conditions [31,36].

Simulations were conducted for July 19, 2022, beginning at 05:00 CET and continuing for 17 h (until 22:00 CET). This date was chosen because Europe experienced one of its most severe heatwaves that year, with Germany being heavily impacted [37]. Meteorological data from Düsseldorf Airport Station supported the selection of July 19, 2022, as the simulation day [38]. This date was at the peak of the heatwave, characterized by high-pressure atmospheric conditions and stable, cloud-free skies over the region, resulting in intense surface heating (Fig. 3). Fig. 3 displays the surface synoptic weather chart issued by the German Weather Service (DWD) at 00:00 UTC, confirming the dominance of an anticyclonic system over Central Europe during the selected period [39].

The simulation used full forcing from observed meteorological data recorded at Düsseldorf Airport Station, including solar radiation (downward direct and diffuse shortwave radiation), air temperature, relative humidity (RH), wind speed and direction.

The spatial resolution of the ENVI-met model was set at 3 m. This value is commonly adopted in ENVI-met applications at the neighborhood scale as a compromise between resolving street-canyon and tree-crown geometry and keeping simulation times computationally manageable [26]. A 63-meter buffer zone was applied to cover the whole study area of interest (within the red line in Fig. 2). To further capture edge interactions, the full simulation area extended at least 100 m beyond the target study area in all directions.

UTCI was calculated using the Biomet post-processing module of ENVI-met, which applies a thermophysiological model to assess outdoor thermal comfort. The input parameters included T_{mrt}, air temperature (T_a), RH and wind speed (v), enabling the evaluation of pedestrian thermal stress across different outdoor locations. We used the default value of pedestrians in the model: a 35-year-old man, 1.75 m tall, with a weight of 75 kg, walking (1.34 m/s).

Building geometry and construction details for ENVI-met and also CitySim were taken from an urban archetype dataset previously developed for Düsseldorf [23]. This dataset provides layer-wise constructions and U-values for the main TABULA residential archetypes and their retrofitted counterparts (see Tables A1 and A3 in Yu et al. [23]). This insulation reduces heat transfer and improves both energy efficiency and thermal comfort. While these measures are designed to reduce winter heat loss, they can alter summer outdoor thermal conditions by reducing inward heat flux and elevating surface façade temperatures, which in turn affects T_{mrt} and pedestrian-level thermal comfort. The main thermophysical and radiative properties (λ, ρ, c_p, α and albedo A, ε) of the envelope and surface materials are summarized in Table 1.

Urban green elements were integrated based on publicly available data from Düsseldorf's tree database [35]. The area includes 262 individual trees, primarily Plane, Lime, and Hornbeam species. Tree heights range from 5–20 m, with crowns of 6–8 m diameter. Both street and garden trees were modeled explicitly in ENVI-met. Within ENVI-met, these trees were represented using the standard deciduous broadleaf parameterizations. This includes default summer Leaf Area Density (LAD) profiles (typically peaking in the mid-canopy) and phenological settings corresponding to full-leaf conditions in July, ensuring that evapotranspiration and shading effects were simulated based on established model defaults.

2.3. Scenario design

Four simulation scenarios were designed for this study at 14:00 CET when UTCI values reach their peak, corresponding to the highest heat stress experienced by urban pedestrians. These include combinations of existing vs. retrofitted buildings and with vs. without vegetation.

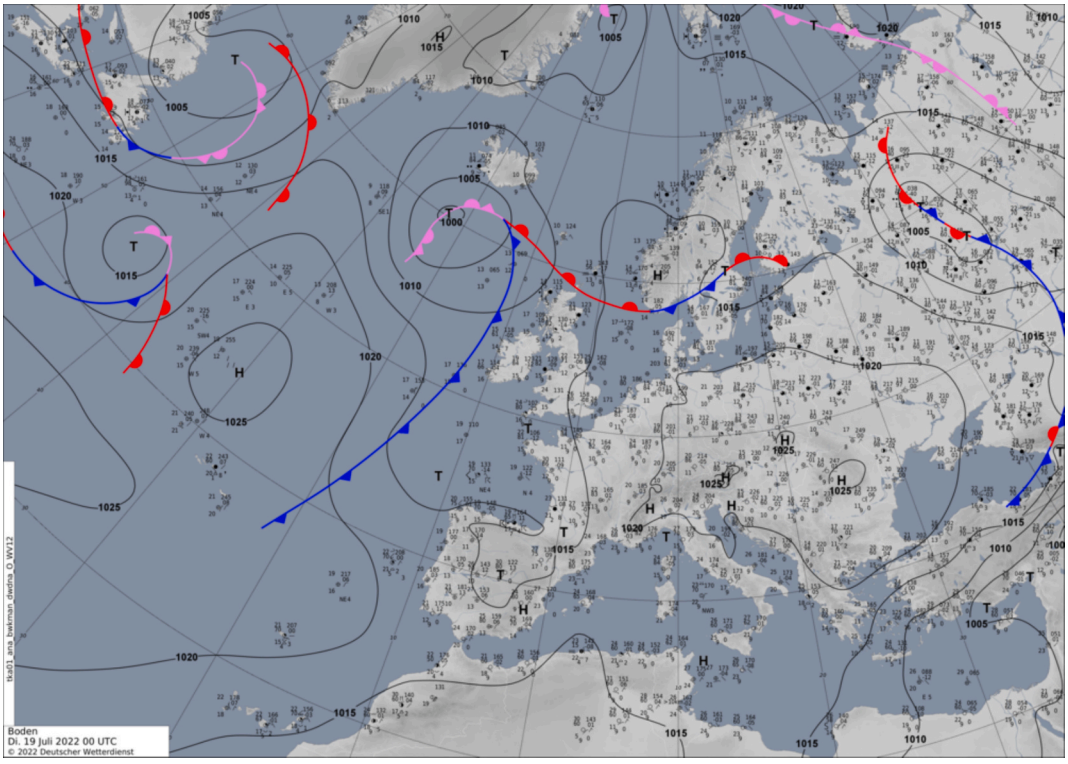


Fig. 3. Surface Synoptic Weather Map during the July 2022 Heatwave in Europe (00 UTC, July 19).) .
Source: Deutscher Wetterdienst (DWD), via Wetterzentrale (https://www.wetterzentrale.de[39]

Table 1
Thermophysical (λ, ρ, c_p) and radiative (α or albedo A, ε) properties of the main envelope and surface materials.

Building Materials						
Type	Material	λ (W/(m·K))	ρ (kg·m^{-3})	c_p (J/(kg·K))	α	ε
Masonry	Solid brick	0.44	1500	650	0.7	0.93
Masonry	Hollow brick / block	0.3	930	840	0.7	0.94
Masonry	Light honeycomb brick	0.2	620	840	0.7	0.94
Masonry	Structural concrete	1.6	2220	850	0.7	0.9
Insulation	Generic external insulation board	0.07	400	1500	0.5	0.9
Plaster	ENVI-Met default plaster	0.6	1500	850	0.6	0.93
Roof	Tile	0.84	1900	800	0.7	0.93
Roof	PVC	0.19	1200	1470	0.3	0.9
Surface Materials						
Type	Material	A	ε			
Pavement	Asphalt	0.12	0.9			
Pavement	Asphalt red	0.4	0.9			
Pavement	Concrete	0.3	0.9			
Pavement	Single stones	0.35	0.9			
Soil	Loamy soil	0.2	0.9			
Vegetation	Grass	0.2	0.97			

*Thermal Conductivity: λ (W/(m·K)); Density: ρ (kg·m^{-3}); Specific Heat: c_p (J/(kg·K)); Absorption: α; Albedo:A; Emissivity: εFor surface materials, the user interface only exposes radiative properties (albedo and emissivity); bulk thermophysical properties are taken from ENVI-met's internal defaults. All volumetric properties of asphalt, concrete and soil surfaces therefore follow the ENVI-met standard database.

Specifically, Scenario A represents the baseline condition of existing buildings with current urban vegetation, while Scenario B simulates existing buildings with vegetation removed. Scenario C incorporates retrofitted building envelopes with retained vegetation, and Scenario D combines retrofitted buildings with no vegetation. Each scenario was designed to isolate and examine the effects of key urban design elements.

T_a (°C), T_{mrt} (°C), RH (%), and v (m/s) were selected as key microclimatic variables because they directly influence human thermal comfort as represented by UTCI (°C). By analyzing these factors, we can better understand how different urban configurations and interventions affect the thermal environment.

We deliberately restricted the scenario set to combinations of standard TABULA-based envelope retrofits and the presence or absence of urban greenery in order to focus on widely implemented, policy-relevant measures and to control the overall computational load. More exploratory configurations, such as reflective surfaces or adaptive natural ventilation strategies, are prioritized for future work rather than being included in the present analysis.

2.4. Outdoor–Indoor simulation using a One-Way ENVI-met–CitySim integration

To assess whether building retrofits optimized for winter efficiency may compromise indoor thermal safety during summer heatwaves, we conducted a simulation using CitySim to simulate effective indoor temperatures under realistic outdoor microclimate conditions.

CitySim cannot directly simulate vegetation surrounding shading elements such as trees. To overcome this limitation and account for green infrastructure effects, we used high-resolution ENVI-met simulation results from two scenarios: Scenario A (existing, non-retrofitted buildings with green space) and Scenario C (retrofitted buildings with green space).

From both ENVI-met simulations, we extracted average hourly outdoor climate variables, including T_a, RH, v and wind direction, for July 19th, 2022, a peak day during the 2022 Central European heatwave. These values were used for the period 05:00–22:00 CET, when ENVI-met was actively simulated. For the remaining hours of the day (00:00–04:00 and 23:00 CET), the original observations from Düsseldorf Airport Station were retained. The resulting mixed profiles were then reformatted to serve as customized weather input profiles for CitySim, replacing standard meteorological files. Radiation inputs (beam and diffuse) were preserved from the original dataset to ensure consistency and to avoid double-counting shading effects, as CitySim already accounts for solar obstruction due to building geometry but does not model vegetation-induced shading. Our analysis of UTCI and indoor temperatures focuses on the common simulation window between both models (06:00–22:00 CET), when ENVI-met-derived microclimate fields are available; earlier and later hours mainly provide thermal preconditioning and are not interpreted in detail.

Indoor simulations were then performed on a representative building typology in two conditions: a non-retrofitted existing building using Scenario A climate data and a retrofitted building using Scenario C climate data. Each building was assigned standard occupant schedules and no active cooling, aligning with common practice in Central European residential buildings. This ensures that the model would simulate the actual passive indoor temperature without artificial truncation. CitySim does not model windows as independent operable elements. Instead, window-related effects are represented indirectly through facade-level parameters such as glazing ratio and solar heat gain coefficient (g-value), which control solar gains but not dynamic ventilation behavior [40,41]. We therefore interpret the resulting indoor temperatures as a conservative "closed window, no-cooling" worst-case estimate of overheating risk.

2.5. Analysis Methodology

Before analyzing the outdoor thermal comfort outcomes across the four design scenarios, we first examined whether the level of detail in building data has an influence on simulated UTCI results. Specifically, we compared a realistic setting based on detailed building archetypes derived from the EU TABULA dataset with ENVI-met's default building setting, where all buildings are treated as having the same genetic material and structure.

The comparison was conducted for Scenarios A and B, which differ only in urban greenery but share identical building layouts. In both cases, we compared UTCI values at 14:00 CET and at a height of 1.5 m. This height corresponds to average human breathing level and is widely accepted for thermal comfort assessments [28]. The goal was not to determine which configuration is more accurate, since no observational validation data are available but to examine whether using realistic building data results in materially different microclimatic outcomes.

Then, to evaluate the effects of different urban design strategies on outdoor thermal comfort, we conducted a statistical analysis of the simulated microclimate data. We extracted UTCI and four key microclimatic variables (T_a, T_{mrt}, RH, and v) at 1.5 m height from 6,032 raster cells within the defined study area (within the red boundary in Fig. 2). These raster data were used to compute area-averaged UTCI values at 2-hour intervals from 06:00 to 22:00 CET under four predefined scenarios (A, B, C, and D). Meanwhile, paired t-tests were used to compare UTCI values between key scenario pairs at 14:00 CET [42](Field, 2013). Specifically, (i) A vs. B for the effect of urban green, (ii) C vs. D for the effect of urban green after retrofit, (iii) B vs. D for the effect of renovation alone. Prior to hypothesis testing, the Shapiro-Wilk test was used to verify the normality of the data, and Levene's test was used to assess the homogeneity of variances [43,44]. Benjamini-Hochberg (BH) corrections were applied where necessary to adjust for multiple comparisons and control the false discovery rate [45].

Next, to quantify the relative impact of each environmental variable on UTCI, we performed ridge regression analysis using four standardized predictor variables (T_a, T_{mrt}, RH, and v) for each scenario [46]. Ridge Regression was selected because it mitigates the strong multicollinearity

especially between T_a and T_{mrt} that is typical under heatwave conditions while retaining all predictors in the model. This method introduces a regularization parameter (α), which stabilizes coefficient estimates, prevents overfitting, and improves model robustness by applying shrinkage to less-influential variables. All input variables were standardized prior to regression to ensure coefficient comparability. The optimal α values were determined automatically via cross-validation for each scenario [47]. For each model, we report: R^2 values; standardized regression coefficients; variance inflation factors (VIFs); and variable weights. The purpose of this analysis is explanatory rather than predictive: ridge regression is used here as a robust regularized regression tool to rank the influence of T_a, T_{mrt}, RH and v, rather than to compare alternative multivariate techniques (e.g. partial least squares).

To further examine the spatial variability of microclimatic influences on thermal comfort, we selected three representative site pairs (six observation points in total) for detailed analysis. Pair 1 is located within a street park, with one observation point situated in the park grass area (Point 1) and the other in the shade of the main road trees (Point 2). Pair 2 is positioned in a neighborhood, with one observation point strategically placed in an open area exposed to direct sunlight (Point 3) and another beside a tall building offering shade (Point 4). Pair 3 spans across a road, with one point on the north side (sun exposed) (Point 5) and another on the south side (shadowed) (Point 6). Fig. 4 illustrates the spatial arrangement of these observation sites.

3 . Results And discussion

3.1. Necessity of realistic building dataset

The spatial UTCI differences between simulations using the TABULA-based realistic building settings (Scenarios A and B) and the ENVI-met default building settings are presented in Fig. 5. The figure illustrates both positive and negative UTCI deviations resulting from the use of realistic building data. Scenario B, which lacks urban green, exhibits a larger UTCI difference compared to Scenario A. The maximum UTCI difference reaches 1.46 °C. The difference is particularly evident in densely built areas with high surface exposure, where realistic material and envelope variations alter the simulated heat storage and radiation balance. These findings demonstrate that the level of building detail plays a critical role in outdoor thermal simulation and can materially affect thermal comfort assessments. The magnitude of modeled differences (e.g., 1.5 °C UTCI sensitivity to archetype realism) is comparable to or larger than reported inter-model variability in ENVI-met-based studies, supporting the robustness of the relative findings.

3.2. Indoor thermal performance under heatwave conditions

Fig. 6 presents the hourly average indoor temperatures of all buildings in research area both their original and retrofitted states on July 19, 2022, the peak of the heatwave. The external meteorological temperature from the Düsseldorf Airport Station is shown as dashed line. This allows us to assess potential unintended indoor consequences of winter-focused retrofits during summer extremes. In line with the modelling setup described in Section 2.4, the interpretation below focuses on the daytime period between approximately 06:00 and 22:00 CET, when the indoor simulations are driven by ENVI-met-derived local microclimate. Hours outside this window mainly provide thermal preconditioning.

The results reveal a clear "crossover pattern." During the late evening and early morning (roughly 22:00–07:00 CET), the retrofitted buildings (blue line) are slightly cooler than the existing stock (orange line). However, as solar radiation intensifies, this advantage quickly reverses. From late morning to evening (about 08:00–21:00 CET), retrofitted buildings exhibit consistently higher indoor temperatures. Starting around 08:00 CET, indoor temperatures in both typologies rise; however, the retrofitted building exhibits a significantly sharper temperature increase, finally reaching a much higher peak. The maximum difference exceeded 3.8 °C around 15:00 CET, pushing the absolute peak indoor temperature to approximately 36.8 °C.

This extreme overheating confirms the severity of the "closed window" worst-case scenario described in Section 2.4. Such temperatures far exceed typical adaptive comfort limits (e.g., 26 °C to 28 °C) and pose a serious health risk to occupants, demonstrating the danger of relying on envelope retrofits without integrating night ventilation or active cooling strategies.

This behavior aligns with fundamental building physics. Retrofitted buildings typically have thicker insulation and reduced air permeability,



Fig. 4. The location of six observation points. The land cover map is consistent with Fig. 2.

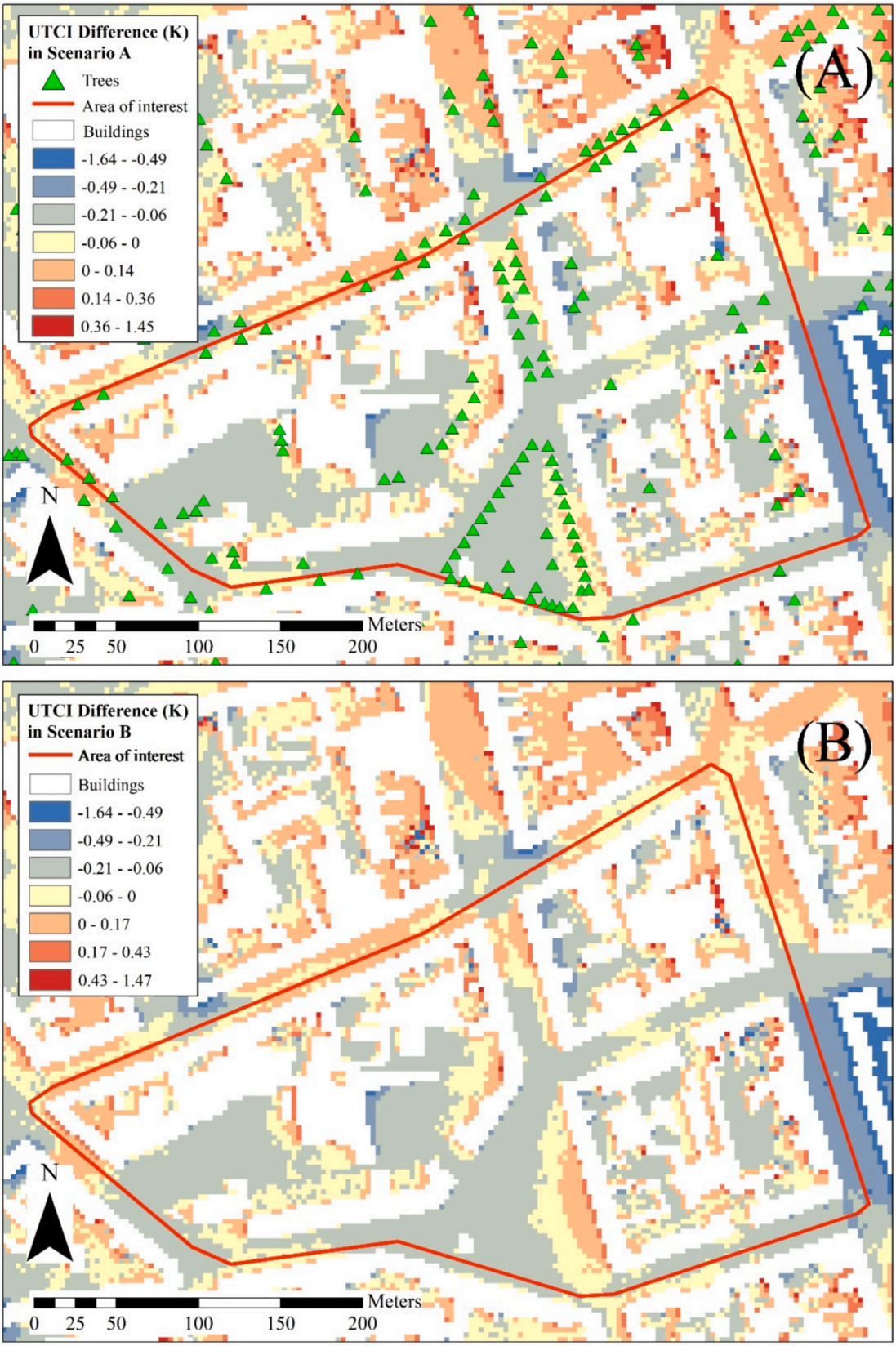


Fig. 5. UTCI difference map at 14:00 CET, 1.5 m height. (A) difference between Scenarios A with Tabula building setting and with ENVI-met default building setting (Tabula setting − default setting), (B) difference between Scenarios B with Tabula building setting and with ENVI-met default building setting. Solar azimuth was 189.49° and solar elevation 59.2°.

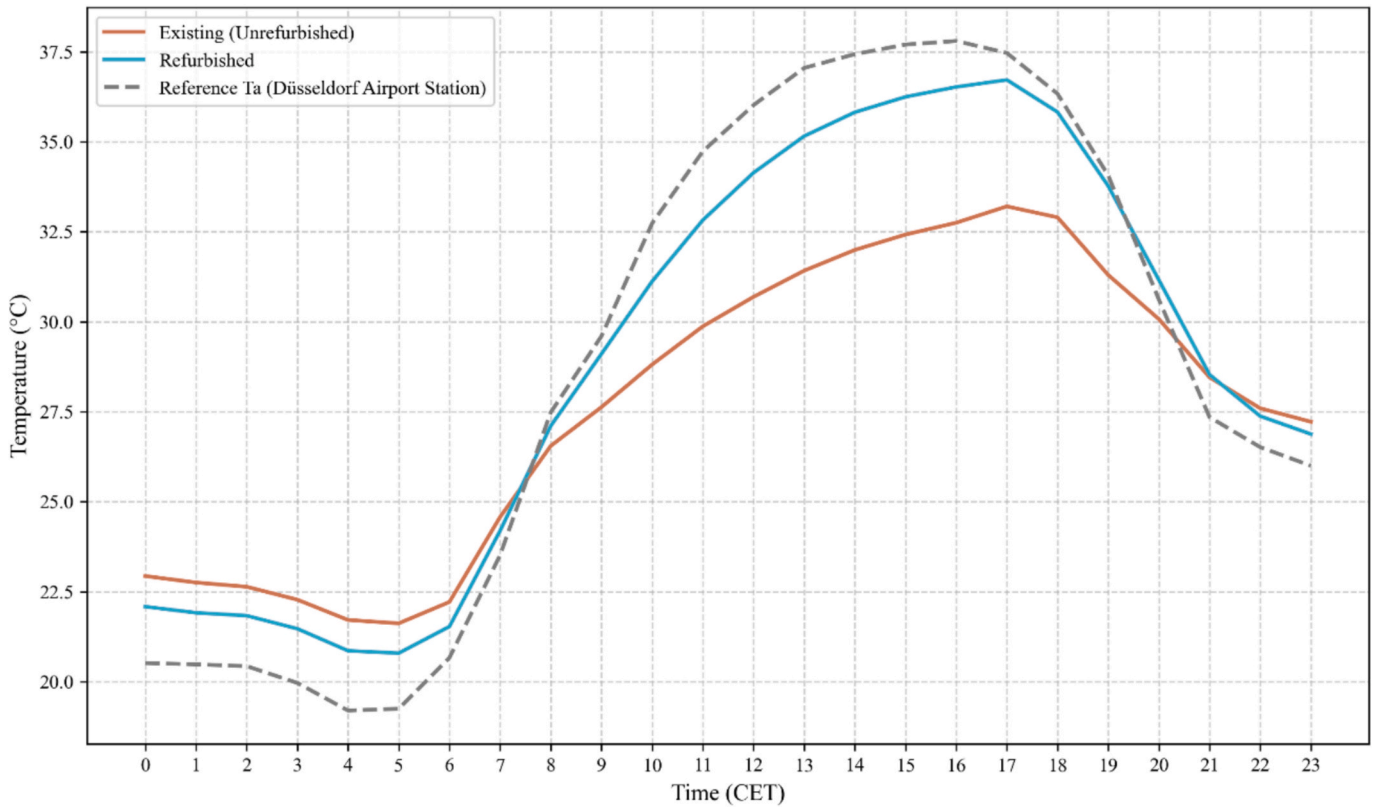


Fig. 6. Hourly average indoor air temperatures (T_a) for all buildings in their existing and retrofitted states on July 19, 2022. The dashed line represents the reference external meteorological temperature, sourced from the Düsseldorf Airport Station. The solid lines represent the simulated indoor conditions in the dense study neighborhood.

which significantly slows heat transfer through the envelope. Combined with improved airtightness, which limits unintentional air exchange, retrofitted buildings begin the day with slightly higher internal temperatures. In the absence of active cooling and limited ventilation (as assumed here, in line with typical Central European housing), once solar radiation enters directly through glazing, governed by the defined glazing ratio and g-value, the retained heat cannot be dissipated effectively, causing the retrofitted buildings to warm more rapidly than the existing ones.

These findings underscore the dual-edged nature of winter-oriented retrofit strategies under extreme summer conditions. While they improve energy efficiency and night-time comfort, they can significantly worsen indoor thermal safety during hot afternoons, particularly in heatwave scenarios and in the absence of adaptive cooling technologies. From a resilience perspective, these results suggest that, under prolonged heatwave conditions and without effective passive or active cooling, retrofitted buildings may struggle to maintain indoor conditions compatible with passive survivability. Specifically, the simulated peak indoor temperatures of approximately 36.8 °C significantly exceed these survivability thresholds, posing severe heat-health risks—particularly for vulnerable populations such as the elderly—who may lack the physiological or technical means to adapt to such extreme internal environments without active cooling.

3.3. Overview of thermal comfort across scenarios

Table 2 summarizes the simulated spatial averages of key climate variables across the entire study area at 14:00 CET across the four scenarios. The UTCI exceeded 41 °C in all scenarios, indicating very strong heat stress during the peak of the heatwave. According to the UTCI stress assessment scale [27], values between 38 °C and 46 °C fall within the 'very strong heat stress' category, posing significant health risks to pedestrians. Scenario B recorded the highest UTCI (43.70 °C), while Scenario C showed the lowest (41.45 °C). T_{mrt} ranged from 55.43 °C in Scenario C to 63.21 °C in Scenario B, confirming the dominance of radiative heat in shaping thermal conditions. T_a remained consistently high across scenarios (>37 °C), averaging between 37.85 °C and 38.25 °C. RH stayed extremely low (21.39–21.95%), which is a result of this hot, dry summer afternoon. The domain-average simulated pedestrian-level wind speed v at 1.5 m height was 0.49 m/s in all four scenarios at 14:00 CET (Table 2). This similarity arises because the tested design changes (building insulation and the presence or absence of trees) had a limited impact on the bulk airflow momentum passing through the domain boundaries. However, local sheltering and turbulence, and channeling effects around buildings and trees were fully resolved at the grid-cell level. These localized variations are reflected in the spatial heterogeneity of the UTCI distribution (discussed in Section 3.6) rather than in the aggregated domain-average value.

Table 2
ENVI-met simulated average values of climatic parameters across four scenarios at 14:00 CET in the study area.

	Scenario A	Scenario B	Scenario C	Scenario D
UTCI (°C)	42.03	43.70	41.45	43.11
T_{mrt} (°C)	56.93	63.21	55.43	61.64
T_a (°C)	38.11	38.25	37.85	37.85
RH (%)	21.64	21.39	21.95	21.69
v (m/s)	0.49	0.49	0.49	0.49

Note: Scenario A: Existing + Green; B: Existing + No Green; C: Retrofitted + Green; D: Retrofitted + No Green

Fig. 7 illustrates the average UTCI values of the whole interest study area (within the red boundary in Fig. 2) under four different scenarios, measured from 06:00 CET to 22:00 CET. Across all scenarios, UTCI values reach their maximum at 14:00 CET, coinciding with the period of

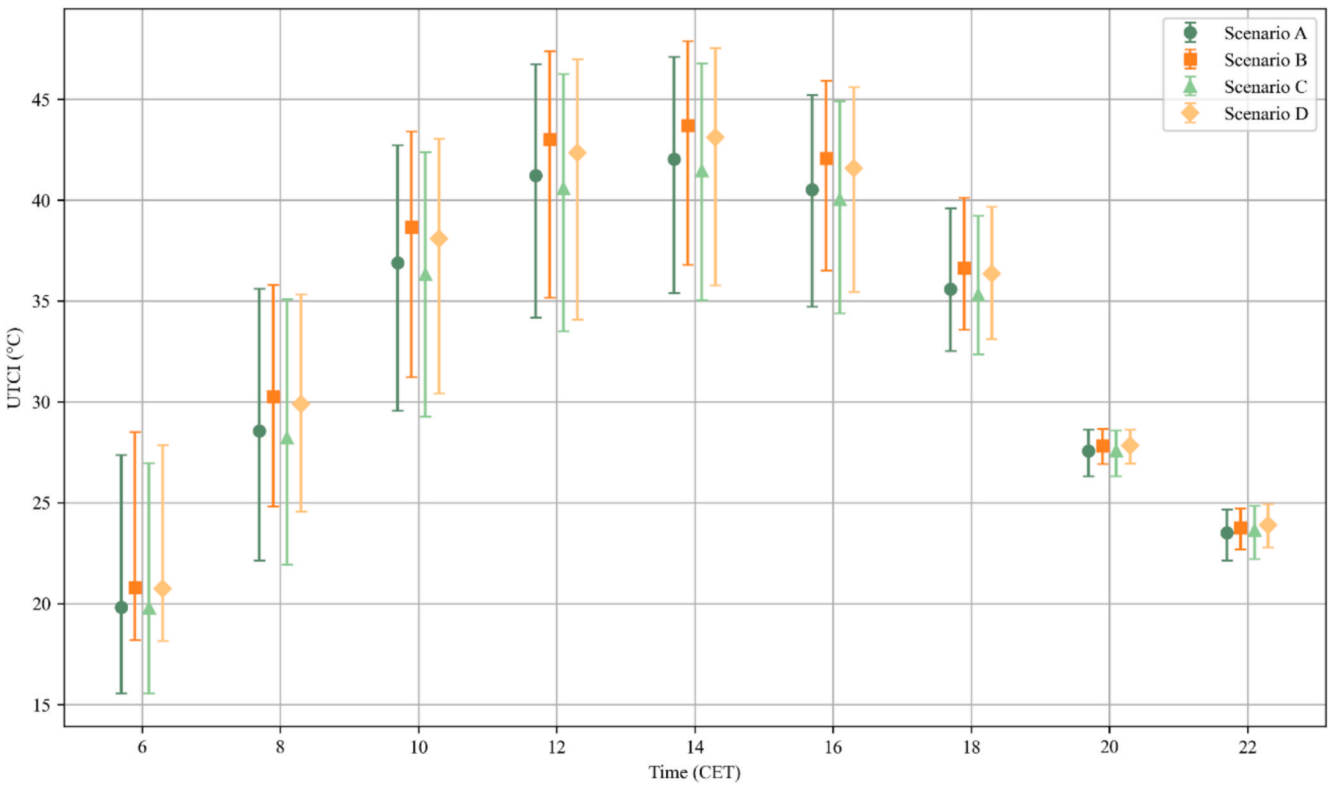


Fig. 7. Hourly average UTCI values (06:00–22:00 CET) across four urban design scenarios (A–D), with vertical error bars representing the minimum and maximum values across 6,032 raster cells.

highest heat stress. At this peak hour, Scenario B exhibits the highest average UTCI (43.70 °C), followed by Scenario D (43.11 °C), Scenario A (42.03 °C), and Scenario C (41.45 °C). The maximum UTCI values range from 46.75 °C to 47.87 °C, with the lowest values (35.02 °C to 36.79 °C), as indicated by the vertical error bars. By 06:00 CET, the start of the simulation period, average UTCI values range from 19.82 °C to 20.89 °C across the scenarios. All scenarios converge to similar UTCI levels (approximately 23.6 °C) by 22:00 CET.

Notably, Scenario C shows the lowest UTCI values across all hours, indicating the effectiveness of combining building retrofit with urban green infrastructure. The UTCI values of Scenarios B, D, and A fall between the two, in descending order.

Fig. 8 illustrates the distribution of UTCI at 1.5 m height for Scenario A and Scenario B at 14:00 CET, the time of day when UTCI peaked. Scenario A and B were selected as representative cases to assess the influence of existing building conditions in combination with and without urban green on localized outdoor thermal comfort.

The results highlight the important roles of tree coverage and building heights in shaping the local microclimate. In Scenario A (Fig. 8 left), UTCI values range from a cooler 34.91 °C in vegetated or shaded areas to a peak of 50.14 °C in sun exposed open spaces. Compared to Scenario B (Fig. 8 right), which lacks vegetation, the overall presence of green in Scenario A reduces the average UTCI by 1.67 °C at peak hour. These microclimatic dynamics show the importance of urban morphology and landscape design in mitigating heat stress.

3.4. *Scenario-specific impacts on outdoor thermal comfort*

To further investigate how specific combinations of building retrofitting measures and urban green infrastructure affect localized outdoor conditions, we conducted statistical tests to compare UTCI values at 14:00 CET, the hottest period of the day. All data met the assumptions of normality and homogeneity of variances, as confirmed by the Shapiro-Wilk and Levene's tests (see Section 2.5). Paired t-tests were applied,

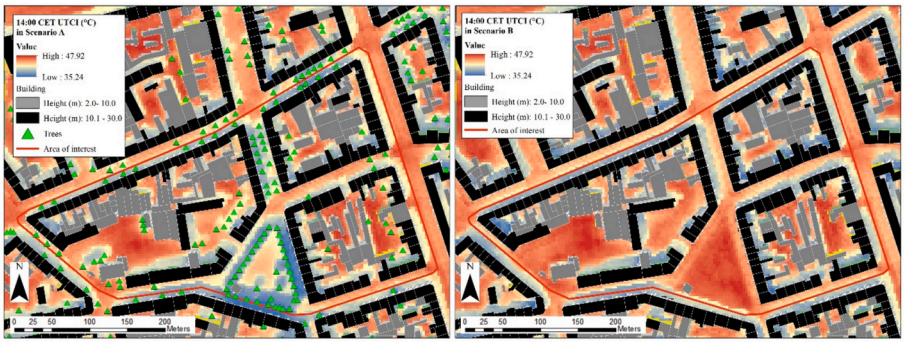


Fig. 8. The 14:00 CET UTCI map of the study area (1.5 m height) of Scenario A (left) and Scenario B (right). The trees' locations in and surrounding the study area are represented by green triangles. Solar azimuth was 189.49° and solar elevation 59.2°. (For interpretation of the references to colour in this figure legend, the reader is referred to the web version of this article.)

and Benjamini-Hochberg correction was used to adjust for multiple comparisons.

The results (Table 3) indicate that all comparisons yielded statistically significant differences ($p < 0.05$ after BH correction); however, the physical relevance differed: nature-based greening produced several-degree changes in UTCI, whereas envelope-only retrofits resulted in sub-degree differences (<1 °C). Specifically, urban green significantly reduced UTCI both before and after retrofit, as seen in Scenarios A and C in Fig. 7, which exhibited the lowest UTCI values at 14:00 CET. Even without vegetation, building retrofit (Scenario D) significantly reduced UTCI compared to the un-retrofitted, non-green Scenario B ($p < 0.05$). In this case, the average UTCI was slightly lower in Scenario D (43.11 °C) than in Scenario B (43.70 °C). However, despite its statistical significance due to consistent directional changes across the domain, this 0.6 °C reduction is physically marginal in the context of extreme heatwaves, as it fails to shift the outdoor thermal environment out of the 'very strong heat stress' category (>41 °C). This should therefore be interpreted as indicating the direction and relative sensitivity of outdoor thermal stress to envelope changes, rather than as a large mitigation effect. By contrast, vegetation produces substantially stronger cooling (>5 °C), highlighting that greenery is the dominant factor for reducing outdoor heat stress in this compact neighborhood. This reduction may be attributed to the altered building envelope properties, which affect how solar radiation is absorbed and reradiated to the surroundings.

3.5. Regression analysis of climatic drivers affecting UTCI

To understand the drivers of outdoor discomfort, ridge regression was performed using the standardized predictor variables T_a, T_{mrt}, RH, and v as predictors, which described in Section 2.5. Table 4 shows the results at 14:00 CET (>37 °C), which further quantifies the influence of climatic parameters on UTCI across the four scenarios. In all cases, the models demonstrated excellent performance, with coefficients of determination ($R2$) consistently above 0.995, indicating that these four parameters sufficiently capture the variance in UTCI values.

T_{mrt} is the dominant factor across all scenarios, with standardized coefficients ranging from 2.371 to 2.608 and accounting for over 91% of the total model weight in all cases. This confirms that radiative heat exchange, strongly influenced by surface properties and shading, is the most critical factor governing outdoor heat stress during summer heatwaves. T_a showed positive but much smaller coefficients, contributing less than 5.2% to the total model weight in all scenarios. While high T_a exacerbates thermal discomfort, its marginal effect is limited once T_{mrt} is already elevated.

RH showed weak and consistently negative coefficients. This issue is particularly evident in Scenarios A and C, where both urban green and extremely low humidity levels are present. In these scenarios, severe multicollinearity was observed between RH and T_a, as reflected by high VIF values exceeding 14. VIF quantifies how strongly a predictor is correlated with other predictors. A high VIF indicates that the variable's coefficient may be unstable due to shared information with other variables. Here, vegetation likely increases RH through evapotranspiration while simultaneously reducing T_a and T_{mrt} due to shading and latent cooling, causing these variables to become highly interdependent. Furthermore, under dry atmospheric conditions, RH and T_a are naturally inversely related. Although ridge regression reduces the distortion from multicollinearity by introducing a small amount of bias into the regression coefficients [48], RH's relative weight in the model remained minor, which is below 3.4% in all cases. Given the strong correlation between Ta and RH and the resulting high VIF values, the corresponding coefficients should be interpreted with caution; however, across all scenarios the dominance of T_{mrt} remains stable.

In contrast, v exhibited a small but positive association with UTCI in all scenarios, with coefficients around 0.078–0.087 and weights around 3%. This observed positive correlation aligns with physiological findings documented by Bröde and Kampmann [49], who noted that UTCI captures both the convective and evaporative heat-transfer effects of wind and wind speed may aggravate thermal strain under extremely hot and dry conditions.

Taken together, these findings confirm that T_{mrt} is the main factor through which urban design interventions, such as tree shading or building insulation can influence outdoor comfort. The limited contribution of RH and v under the simulated conditions highlights the dominance of radiative effects over convective or latent heat exchanges during extreme afternoon heat.

To assess how these parameter-level effects translate into real-world mitigation strategies, the next section examines scenario-specific impacts on UTCI across the study area.

Table 3
Paired t-Test results for UTCI differences across urban design and retrofitscenarios at 14:00 CET, with BH correction.

Scenario Comparison	Tested Impact Factor	t-Statistic	Raw p-Value	BH Corrected p-Value	Significance level
A vs. B	Effect of greening	−5.84	0.0004	0.0008	Highly Significant ($p < 0.01$)
C vs. D	Effect of greening after retrofit	−5.88	0.0004	0.0008	Highly Significant ($p < 0.01$)
B vs. D	Effect of building renovation	3.28	0.0112	0.015	Significant ($p < 0.05$)

Table 4
Ridge regression analysis of urban design and climatic factors impacting UTCI at 14:00 CET across different scenarios.

Scenario	Parameters	R2	Standardized Coefficient	Collinearity Statistics (VIF)	Weight (%)
A	T_{mrt}	0.996	2.580	1.231	91.7
	T_a	0.996	0.131	16.888	4.7
	RH	0.996	−0.019	17.579	0.7
	v	0.996	0.083	1.403	3
B	T_{mrt}	0.996	2.371	1.154	92.3
	T_a	0.996	0.053	8.052	2.1
	RH	0.996	−0.058	7.901	2.3
	v	0.996	0.087	1.257	3.4
C	T_{mrt}	0.996	2.608	1.280	91.6
	T_a	0.996	0.148	14.514	5.2
	RH	0.996	−0.008	14.810	0.3
	v	0.996	0.085	1.394	3
D	T_{mrt}	0.996	2.501	1.214	92.3
	T_a	0.996	0.029	2.425	1.1
	RH	0.996	−0.092	2.000	3.4
	v	0.996	0.087	1.807	3.2

Note: The α values used in the ridge regression were selected automatically through cross-validation, and were 0.201 (A), 0.050 (B), 0.175 (C), and 0.066 (D), respectively.

3.6. Localized impacts of microclimate variables on UTCI

To enhance our understanding of how microclimate variables influence thermal comfort at a localized level, we selected three pairs comprising a total of six observation sites (see Section 2.5). Each pair highlights different urban morphologies and degrees of exposure to vegetation and building shading. For each location, we analyzed UTCI and T_{mrt} at 14:00 CET, the hour of maximum thermal stress across the four design scenarios (Fig. 9). Wind speed, while locally variable, is discussed textually due to its complex spatial dynamics and to maintain visual clarity. T_a and RH were excluded from localized graphical analysis due to their relatively low spatial and statistical variability (see Sections 3.4 and 3.5).

Points 1 and 2 are located in the park area with urban green under

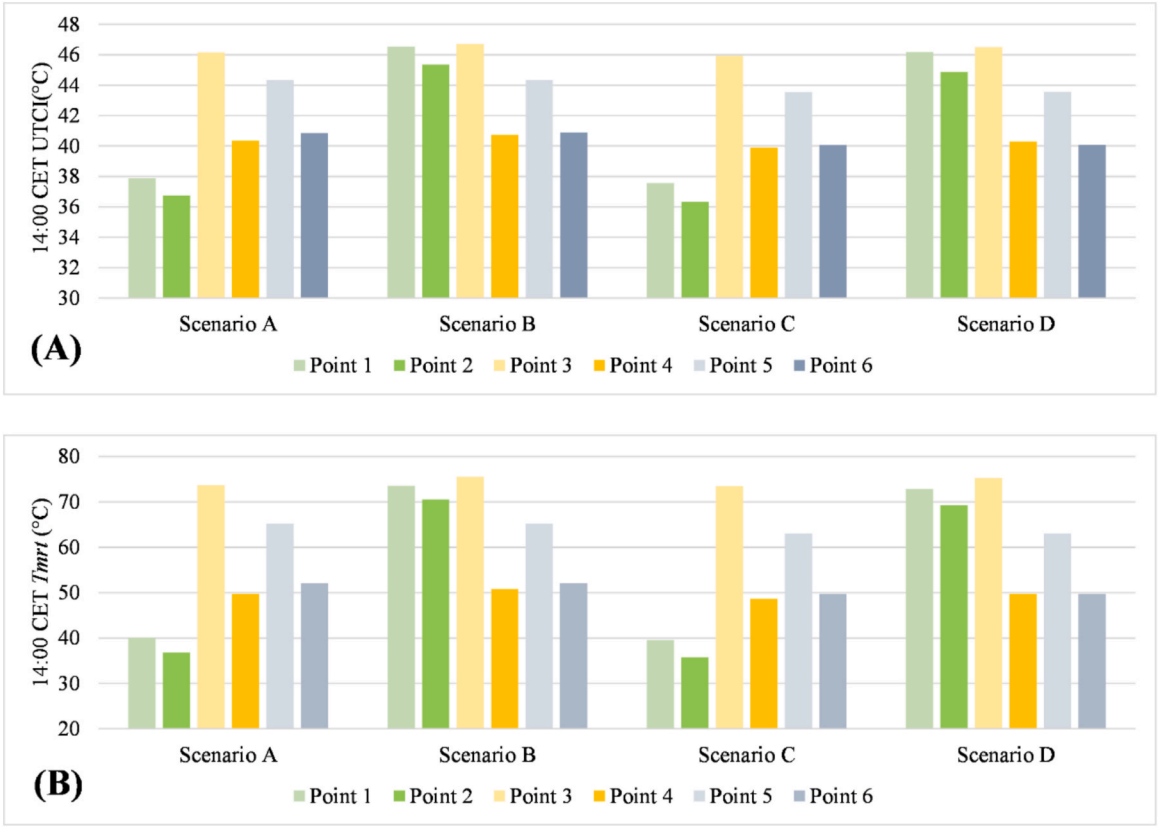


Fig. 9. UTCI values (A) alongside variations in T_{mrt} (B) across four scenarios at 14:00 CET for six observation points within the study area.

scenarios A and C, consistently showing the lowest UTCI values. In scenarios lacking urban green (B and D), UTCI increases greatly by over 5 °C at 14:00 CET due to full solar exposure. Among these, point 2, which is slightly closer to an adjacent tall building, shows slightly lower UTCI value than point 1. Points 3 and 4 are situated within a block lacking urban green and display significant differences in UTCI values (about a 6 K difference in all scenarios). Point 3 is located in an open area without any vegetation and fully exposed to sunlight and consistently shows the highest UTCI values across all scenarios. The presence of tall buildings around point 4 casts shadows that substantially cool the area and leads to this notable difference between the two points. Points 5 and 6 are positioned on opposite sides of a street, near tall buildings with sparse vegetation. Buildings provide shading that beneficially lowers UTCI on the south side (Point 6) compared to the north side (Point 5), with a difference of approximately 3.5 °C.

Across all points, T_{mrt} closely mirrored UTCI trends, confirming the strong positive correlation observed in the ridge regression analysis (Section 3.4). Areas with effective shading from trees or building geometry exhibited significantly lower T_{mrt}, translating into better thermal comfort. Conversely, open, sun-exposed areas showed peak values for both T_{mrt} and UTCI. Meanwhile, Scenario D, only with building retrofit moderately reduces UTCI (ranging 0.24——0.82 °C for each Point) compared to Scenario B. While consistent, this limited cooling effect confirms that envelope retrofits alone are insufficient to mitigate heat stress without the complementary shading provided by vegetation.

In comparison, T_a and RH showed minimal spatial variation across observation points and contributed little explanatory value. These findings are consistent with the regression results, which attributed less than 5% of model weight to T_a and under 3.4% to RH in all scenarios. v varied more noticeably among locations, with open areas such as Point 3 experiencing the highest values (>1.34 m/s), while more sheltered points (1, 2, 5, and 6) recorded the lowest. However, even in breezier areas, the dominant influence of radiation outweighed the modest cooling effect of wind under these dry, hot conditions.

These localized findings emphasize the crucial role of shading and surface radiation exchange in shaping outdoor thermal comfort, especially during heatwave conditions. They also support the broader simulation results: combining building retrofits with green infrastructure provides the most effective strategy for mitigating heat stress in urban environments.

4 . Conclusion

This study evaluated the summer thermal implications of EU-standard residential retrofits by integrating realistic TABULA archetypes into a microclimate analysis of the peak day (19 July 2022) of the Düsseldorf heatwave. Validating the importance of envelope realism, the use of specific archetype data produced spatial UTCI differences of up to 1.5 °C compared to generic defaults. Besides, the results quantify a key trade-off between mitigation and adaptation: although green infrastructure reduced peak UTCI by up to 6.0 °C, building retrofits optimized solely for winter energy efficiency inadvertently exacerbated summer risks. Specifically, a “crossover effect” was observed, where under conservative closed window and no cooling conditions, the retrofitted building envelope reduced heating demand but increased indoor daytime peak temperatures by up to 3.8° C. This peak exceeds heat-health guidance for safe indoor temperatures, highlighting potential risks for vulnerable occupants during heatwaves in uncooled dwellings.

These findings verify that T_{mrt}, explaining over 91% of UTCI variance, is the dominant driver of outdoor comfort. This reflects the central role of radiative processes, façade surface temperatures and shading in determining pedestrian heat stress, with trees and other vegetated elements providing both radiative shielding and latent cooling through evapotranspiration. Consequently, for municipal planners and engineers, current EU retrofit policies and practical implementation should look beyond envelope insulation and incentivize “summer-aware”

packages that combine insulation with nature-based solutions and external shading, to prevent locking in indoor overheating risks.

While the proposed framework offers a potentially scalable method for bridging urban microclimate and building energy domains in other TABULA-covered cities, the results must be interpreted within specific modeling limitations. Specifically, the adopted one-way integration prioritizes passive envelope performance and does not represent anthropogenic heat feedback to the microclimate. We also acknowledge inherent limitations in the simulation engines, such as ENVI-met's known tendency to overestimate daytime air temperatures under stable conditions and CitySim's simplified radiation exchange. However, these systematic biases apply across all scenarios, ensuring that the reported relative differences remain stable. Furthermore, the indoor results represent a worst-case scenario for unventilated, uncooled spaces. Finally, since we focused on temperature and index-based indicators (T_a, T_{mrt}, UTCI and indoor air temperature) rather than on sensible and latent heat-flux budgets, a more detailed flux-based energy-balance analysis is therefore left for future work. Based on this work, future research could extend this one-way ENVI-met to CitySim workflow toward fully coupled approaches with site-specific observational validation and conduct systematic uncertainty and sensitivity analyses to refine human-centric retrofit guidelines.

CRediT authorship contribution statement

Qinghua Yu: Writing – review & editing, Writing – original draft, Visualization, Validation, Software, Methodology, Investigation, Formal analysis, Conceptualization. **Gerald Mills:** Writing – review & editing, Visualization, Validation, Supervision, Project administration, Conceptualization. **Gunnar Ketzler:** Writing – review & editing, Supervision, Software, Project administration, Investigation, Data curation, Conceptualization. **Michael Leuchner:** Writing – review & editing, Supervision, Software, Project administration, Funding acquisition, Data curation, Conceptualization.

Declaration of competing interest

The authors declare that they have no known competing financial interests or personal relationships that could have appeared to influence the work reported in this paper.

Acknowledgements

The authors would like to acknowledge funding from China Scholarship Council. The project was partly co-funded under the Excellence Strategy of the Federal Government and the Länder (Project SFBLE003 TRUKLIB).

Data availability

Data will be made available on request.

References

[1] S. Martinez, A. Machard, A. Pellegrino, K. Touili, L. Servant, E. Bozonnet, A practical approach to the evaluation of local urban overheating–a coastal city case-study, Energ. Buildings 253 (2021) 111522, https://doi.org/10.1016/j.enbuild.2021.111522.

[2] S Stewart, I.D.; Mills, G. *The Urban Heat Island—A Guidebook, First Edition*; Elsevier: Amsterdam, The Netherlands, 2021; p. 184. https://doi.org/10.1016/C2017-0-02872-0.

[3] M. Santamouris, Recent progress on urban overheating and heat island research. Integrated assessment of the energy, environmental, vulnerability and health impact. Synergies with the global climate change, Energ. Buildings 207 (2020) 109482.https://doi.org/10.1016/j.enbuild.2019.109482.

[4] J. Coates, K.A. Mar, N. Ojha, T.M. Butler, The influence of temperature on ozone production under varying NO x conditions–a modelling study, Atmos. Chem. Phys. 16 (18) (2016) 11601–11615.https://doi.org/10.5194/acp-16-11601-2016.

[5] N. Aghamohammadi, M. Santamouris (Eds.), *Urban Overheating: Heat Mitigation and the Impact on Health*, Springer.https://doi.org/10.1007/978-981-19-4707-0, Singapore, 2022.

[6] F. Hashemi, G. Mills, U. Poerschke, L.D. Iulo, G. Pavlak, L. Kalisperis, A Novel Parametric Workflow for Simulating Urban Heat Island Effects on Residential Building Energy Use: Coupling local climate zones with the Urban Weather Generator a Case Study of Seven US Cities, Sustain. Cities Soc. 105568 (2024), https://doi.org/10.1016/j.scs.2024.105568.

[7] J. Ballester, M. Quijal-Zamorano, R.F. Méndez Turrubiates, F. Pegenaute, F. R. Herrmann, J.M. Robine, H. Achebak, Heat-related mortality in Europe during the summer of 2022, Nat. Med. 29 (7) (2023) 1857–1866, https://doi.org/10.1038/s41591-023-02419-z.

[8] R. Kraemer, N. Kabisch, Parks under stress: air temperature regulation of urban green spaces under conditions of drought and summer heat, Front. Environ. Sci. 10 (2022) 849965.https://doi.org/10.3389/fenvs.2022.849965.

[9] X. Wang, H. Li, S. Sodoudi, The effectiveness of cool and green roofs in mitigating urban heat island and improving human thermal comfort, Build. Environ. 217 (2022) 109082.https://doi.org/10.1016/j.buildenv.2022.109082.

[10] Y. Hui, Y. Tang, Q. Yang, A. Mochida, Numerical study on influence of surface vegetation on aerodynamics of high-rise buildings, Sustain. Cities Soc. 107 (2024) 105407.https://doi.org/10.1016/j.scs.2024.105407.

[11] Jiang, R., Dong, Y., Bai, L., Dong, W., & Qu, A. (2025). Predicting urban residents' climate change risk perceptions: The role of heat and green space exposure indicators in Harbin's residential environment. *Sustainable Cities and Society*, 106882.https://doi.org/10.1016/j.scs.2025.106882.

[12] J. Xiong, Y. Zhang, M. Han, J. Wu, Z. Tian, Building energy-saving mechanism for indoor cooling temperature set-point with different envelope: a case study in Guangzhou, Journal of Chinese Architecture and Urbanism 5 (2) (2023) 0877. https://doi.org/10.36922/jcau.0877.

[13] Y. Yang, X. Li, Z. Yao, A. Yu, M. Wang, Impact of Facade Photovoltaic Retrofit on Building Carbon Emissions for Residential buildings in Cold Regions, Buildings 15 (20) (2025) 3762.https://doi.org/10.3390/buildings15203762.

[14] C. Cheng, X. Deng, X. Zhao, Y. Xiong, Y. Zhang, Multi-occupant dynamic thermal comfort monitoring robot system, Build. Environ. 234 (2023) 110137, https://doi.org/10.1016/j.buildenv.2023.110137.

[15] K. Ma, Y. Yu, B. Yang, J. Yang, Demand-side energy management considering price oscillations for residential building heating and ventilation systems, IEEE Trans. Ind. Inf. 15 (8) (2019) 4742–4752, https://doi.org/10.1109/TII.2019.2901306.

[16] W. Shang, J. Liu, H. Meng, L. Jia, X. Dai, A RL-based human behavior oriented optimal ventilation strategy for better energy efficiency and indoor air quality, Energ. Buildings 116072 (2025), https://doi.org/10.1016/j.enbuild.2025.116072.

[17] M.C. Peel, B.L. Finlayson, T.A. McMahon, Updated world map of the Köppen-Geiger climate classification, Hydrol. Earth Syst. Sci. 11 (5) (2007) 1633–1644, https://doi.org/10.5194/hess-11-1633-2007.

[18] Verordnung über einen energiesparenden Wärmeschutz bei Gebäuden (Erste Verordnung zur Durchführung des Gesetzes zur Einsparung von Energie in Gebäuden) vom 11. August 1977. *Bundesgesetzblatt I*, 1977, 1554–1564.

[19] E. Mata, A.S. Kalagasidis, F. Johnsson, Contributions of building retrofitting in five member states to EU targets for energy savings, Renew. Sustain. Energy Rev. 93 (2018) 759–774, https://doi.org/10.1016/j.rser.2018.05.014.

[20] T. Loga, B. Stein, N. Diefenbach, TABULA building typologies in 20 European countries—Making energy-related features of residential building stocks comparable, Energ. Buildings 132 (2016) 4–12, https://doi.org/10.1016/j.enbuild.2016.06.094.

[21] The European Parliament and the Council of the European Union, *Directive 2010/31/EU of the European Parliament and of the Council of 19 May 2010 on the energy performance of buildings*, Available at: Off. J. Eur. Union 53 (2010) 13–35 http://eur-lex.europa.eu/LexUriServ/LexUriServ.do?uri=OJ:L:2010:153:0013:0035:EN:PDF.

[22] D. Preziuso, P. Odonkor, Governance gaps in urban decarbonization: Illuminating structural exclusion in residential energy transitions, Energy & Environmental Sustainability 1 (4) (2025) 100054, https://doi.org/10.1016/j.rser.2018.05.014.

[23] Q. Yu, G. Mills, G. Ketzler, M. Leuchner, Developing an urban geographic archetype dataset to support energy retrofit strategy on residential buildings in Düsseldorf, Germany, Energy Rep. 14 (2025) 282–293, https://doi.org/10.1016/j.egyr.2025.06.004.

[24] G. Mutani, S. Coccolo, K. Jérôme, M. Bilardo, CitySim Guide: Urban Energy Modelling. (2018).

[25] T. Vermeulen, J.H. Kämpf, B. Beckers, September). Urban form optimization for the energy performance of buildings using Citysim, in: In *Proceedings of CISBAT*, 2013, pp. 915–920.

[26] Bruse, M. (2004). ENVI-met 3.0: updated model overview. *University of Bochum.* Retrieved from: http://www.envi-met.com.

[27] K. Blazejczyk, Y. Epstein, G. Jendritzky, H. Staiger, B. Tinz, Comparison of UTCI to selected thermal indices, Int. J. Biometeorol. 56 (2012) 515–535, https://doi.org/10.1007/s00484-011-0453-2.

[28] Q. Yu, G. Ketzler, G. Mills, M. Leuchner, Exploring the integration of urban climate models and urban building energy models through shared databases: a review, Theor. Appl. Climatol. 156 (5) (2025) 266, https://doi.org/10.1007/s00704-025-05501-3.

[29] J. Kämpf, S. Coccolo, D. Mauree, J.L. Scartezzini, An integrated microclimate-energy demand simulation method for the assessment of urban districts, Front. Built Environ. 6 (2020) 553946, https://doi.org/10.3389/fbuil.2020.553946.

[30] K. Perini, A. Chokhachian, S. Dong, T. Auer, Modeling and simulating urban outdoor comfort: Coupling ENVI-Met and TRNSYS by grasshopper, Energ. Buildings 152 (2017) 373–384, https://doi.org/10.1016/j.enbuild.2017.07.061.

[31] T. Silva, M. Matias, C. Girotti, J. Vasconcelos, A. Lopes, Heat stress mitigation by exploring UTCI hotspots and enhancing thermal comfort through street trees, Theor. Appl. Climatol. 156 (3) (2025) 162, https://doi.org/10.1007/s00704-025-05400-7.
[32] P.J. Crank, A. Middel, P. Coseo, D.J. Sailor, Microclimate impacts of neighborhood redesign in a desert community using ENVI-met and MaRTy, Urban Clim. 52 (2023) 101702, https://doi.org/10.1016/j.uclim.2023.101702.
[33] City of Dusseldorf, 2023a. Demografiemonitoring 2013 bis 2022 (Statistische Informationen Nr. 320). https://www.duesseldorf.de/fileadmin/Amt12/statistik/stadtforschung/download/Demografiemonitoring_2023_V10_Seite_web_bf.pdf/. (accessed 13 March 2025).
[34] S. Düsseldorf, *Weather stations of the state capital Düsseldorf*, Open Data Düsseldorf. (2022). https://opendata.duesseldorf.de/dataset/wetterstationen-der-landeshauptstadt-d%C3%BCsseldorf.
[35] B. Hofmeister, The study of urban form in Germany, Urban Morphol. 8 (1) (2003) 3–12. https://doi.org/10.51347/jum.v8i1.3908.
[36] B. Song, S.H. Kim, G. Park, K. Park, Comparison of urban physical environments and thermal properties extracted from unmanned aerial vehicle images and ENVI-met model simulations, Build. Environ. 261 (2024) 111705, https://doi.org/10.1016/j.buildenv.2024.111705.
[37] Copernicus, Copernicus: Summer 2022 Europe's hottest on record, Copernicus Climate Change Service/ECMWF. (2022). https://climate.copernicus.eu/copernicus-summer-2022-europes-hottest-record.
[38] C.C. Ibebuchi, I.O. Abu, Characterization of temperature regimes in Western Europe, as regards the summer 2022 Western European heat wave, Clim. Dyn. 61 (7) (2023) 3707–3720, https://doi.org/10.1007/s00382-023-06760-4.
[39] D. Wetterdienst, (dwd),, Surface synoptic weather map of Europe at 00 UTC on 19 July 2022, Retrieved via Wetterzentrale. Available at: https://www.wetterzentrale.de/reanalysis.php?jaar=2022&maand=7&dag=19&uur=000&var=45&map=1&model=dwd (accessed 1 August, 2025, , 2022.
[40] C. Miller, D. Thomas, J. Kämpf, A. Schlueter, Urban and building multiscale co-simulation: case study implementations on two university campuses, Journal of Building Performance Simulation 11 (3) (2018) 309–321, https://doi.org/10.1080/19401493.2017.1354070.
[41] Robinson D., Haldi F. (2009). *CitySim: Comprehensive micro-simulation of resource flows for sustainable urban planning.* Proceedings of IBPSA 2009.
[42] A. Field, *Discovering statistics using IBM SPSS statistics*, (4th ed.)., Sage Publications, 2013.
[43] H. Levene, Robust tests for equality of variances, in: I. Olkin (Ed.), *Contributions to Probability and Statistics: Essays in Honor of Harold Hotelling*, Stanford University Press, 1960, pp. 278–292.
[44] S.S. Shapiro, M.B. Wilk, An analysis of variance test for normality (complete samples), Biometrika 52 (3/4) (1965) 591–611, https://doi.org/10.2307/2333709.
[45] Y. Benjamini, Y. Hochberg, Controlling the false discovery rate: a practical and powerful approach to multiple testing, Journal of the Royal Statistical Society: Series B (methodological) 57 (1) (1995) 289–300. https://www.jstor.org/stable/2346101.
[46] G.C. McDonald, Ridge regression, Wiley Interdisciplinary Reviews: Computational Statistics 1 (1) (2009) 93–100, https://doi.org/10.1002/wics.14.
[47] K.C. Arum, S.C. Ndukwe, H.E. Oranye, O.B. Sule, Comparative analysis of ridge and principal component regression in addressing multicollinearity, FUDMA Journal of Sciences 9 (1) (2025) 240–245. https://doi.org/10.33003/fjs-2025-0901-2981.
[48] C. García García, R. Salmerón Gómez, J. García Pérez, A review of ridge parameter selection: minimization of the mean squared error vs. mitigation of multicollinearity, Communications in Statistics - Simulation and Computation 53 (8) (2022) 3686–3698, https://doi.org/10.1080/03610918.2022.2110594.
[49] P. Bröde, B. Kampmann, Temperature–humidity-dependent wind effects on physiological heat strain of moderately exercising individuals reproduced by the universal thermal climate index (UTCI), Biology 12 (6) (2023) 802, https://doi.org/10.3390/biology12060802.
[50] Landeshauptstadt Düsseldorf, Umweltamt (2022): Baumkataster der Stadt Düsseldorf; downloaded https://fragdenstaat.de/anfrage/baumkataster-der-stadt-dusseldorf/693246/anhang/LHD_Baumkataster_20220428_Ausgang.xlsx, 29.11.2023.